

# Electric field modulation of spin transport F

SCI


Cite as: APL Mater. **10**, 011102 (2022); <https://doi.org/10.1063/5.0073180>


Submitted: 28 September 2021 • Accepted: 16 November 2021 • Published Online: 04 January 2022

 C. Zucchetti,  A. Marchionni,  M. Bollani, et al.

## COLLECTIONS

Note: This paper is part of the Special Topic on Materials Challenges for Nonvolatile Memory.

 This paper was selected as Featured

 This paper was selected as Scilight



View Online



Export Citation



CrossMark

## ARTICLES YOU MAY BE INTERESTED IN

[A New Look at Spin Transport: Spinning a Negative into a Strength](#)

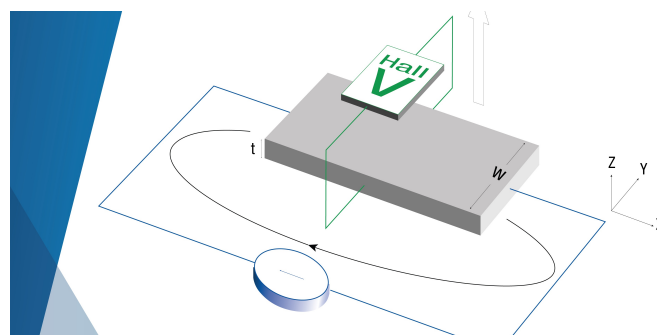
Scilight **2022**, 011104 (2022); <https://doi.org/10.1063/10.0009062>

[Current-induced switching of a ferromagnetic Weyl semimetal  \$\text{Co}\_2\text{MnGa}\$](#)

Applied Physics Letters **119**, 212409 (2021); <https://doi.org/10.1063/5.0073537>

[Role of oxygen migration on the thermal stability of the perpendicular magnetic anisotropy in bottom and top structures](#)

APL Materials **10**, 011101 (2022); <https://doi.org/10.1063/5.0076579>



**Tips for minimizing  
Hall measurement errors**

Download the Technical Note

 **Lake Shore**  
CRYOTRONICS

# Electric field modulation of spin transport

Cite as: APL Mater. 10, 011102 (2022); doi: 10.1063/5.0073180  
Submitted: 28 September 2021 • Accepted: 16 November 2021 •  
Published Online: 4 January 2022



C. Zucchetti,<sup>1,a)</sup>  A. Marchionni,<sup>1</sup>  M. Bollani,<sup>2</sup>  F. Ciccacci,<sup>1</sup>  M. Finazzi,<sup>1</sup>  and F. Bottegoni<sup>1</sup> 

## AFFILIATIONS

<sup>1</sup> LNESS-Dipartimento di Fisica, Politecnico di Milano, Piazza Leonardo da Vinci 32, 20133 Milan, Italy

<sup>2</sup> Istituto di Fotonica e Nanotecnologie del Consiglio Nazionale delle Ricerche, Piazza Leonardo da Vinci 32, 20133 Milan, Italy

**Note:** This paper is part of the Special Topic on Materials Challenges for Nonvolatile Memory.

**a)** Author to whom correspondence should be addressed: [carlo.zucchetti@polimi.it](mailto:carlo.zucchetti@polimi.it)

## ABSTRACT

The finite spin lifetime in solids is often considered a major hindrance for the development of spintronic devices, which typically require cryogenic temperatures to mitigate this phenomenon. In this work, we show that this feature can instead be exploited to realize a scheme where spin transport is modulated at room temperature by a modest electric field. A field directed antiparallel (parallel) to the spin-diffusion velocity can, in fact, largely increase (decrease) the spin-transport length compared with the zero field case. We find that applying an electric field  $E = 24$  V/cm along a  $40$   $\mu\text{m}$ -long path in germanium results in about one order of magnitude modulation of the spin-polarized electrons entering into the detector. This work demonstrates that electric fields can be exploited for guiding spins over macroscopic distances and for realizing fast room temperature modulation of spin accumulation.

© 2022 Author(s). All article content, except where otherwise noted, is licensed under a Creative Commons Attribution (CC BY) license (<http://creativecommons.org/licenses/by/4.0/>). <https://doi.org/10.1063/5.0073180>

The ultimate goal of spintronics is the active control of spin-polarization within a solid-state environment.<sup>1,2</sup> Recently, spin-orbit coupling (SOC) emerged as a promising tool for implementing such a spin manipulation.<sup>3</sup> A large SOC, however, leads to short spin lifetime and diffusion lengths, representing a severe limitation for the development of spintronic devices. Conversely, the small SOC in light semiconductors results in longer electron spin lifetimes, as observed in both lightly doped bulk<sup>4</sup> and low-dimensional materials.<sup>5,6</sup> Among semiconductors, Si and Ge possess the longest lifetimes since, at variance from GaAs, the Dyakonov-Perel mechanism of spin relaxation is totally suppressed in a centrosymmetric lattice.<sup>7</sup> Although Si-based spintronics would be desirable, optically generating non-equilibrium spin populations in lightly doped Si are inefficient compared to Ge.<sup>8,9</sup> Moreover, Ge-based platforms could host spintronic, electronic, and photonic devices, all integrated on a Si-compatible platform. Indeed, the Ge direct gap matches the conventional telecommunication window,<sup>10,11</sup> and the 4% lattice mismatch with Si does not prevent the ready integration of Ge with the mainstream Si-based technology, eventually enabling strain to engineer new functionalities.<sup>12-14</sup>

Within this frame, a relevant feature of a semiconductor spintronic device would be to carry the spin information over long distances. To this aim, spin drift helps in increasing the spin-transport length,<sup>15-17</sup> and variation of the spin-dependent signal upon the application of electric fields has been observed in various contexts.<sup>18-24</sup> Although experimental studies on spin

drift in semiconductors<sup>15-20</sup> have shown that the spin-transport length can be modulated, most of them are performed at cryogenic temperatures<sup>15,17,18</sup> or investigate the effect of electric fields on spin transport only in an indirect way.<sup>16-20</sup>

We have recently proposed a nonlocal spin-injection/detection scheme which enables one to directly image spin transport in a diffusive regime<sup>25,26</sup> and obtain a direct measure of the spin-diffusion length. We employ the same paradigm to investigate drift-diffusive spin transport at room temperature with a device-oriented architecture, showing that a finite spin-diffusion length combined with the application of an electric field can be capitalized to manipulate spin accumulation. The investigated scheme could thus modulate spin transport over long distances and is expected to reach fast timescales. Preliminary simulations obtained from a time-dependent spin drift-diffusion model predict that, for realistic electric field amplitudes, carrier mobility, and spin lifetime, modulation frequencies reaching 10 GHz can be attained, which is much faster compared to other spin accumulation/modulation systems.<sup>27</sup> With respect to previously reported solutions,<sup>15-20</sup> our platform combines all the following characteristics, which make it extremely promising for the development of next generation spintronic devices: (i) room temperature operation; (ii) a large (about one order of magnitude) modulation of spin accumulation; (iii) spin-transport lengths that can be pushed above  $40$   $\mu\text{m}$ ; and (iv) application of moderate control electric fields, which is essential for low power consumption operation.

In particular, we report on the drift-diffusive spin-transport regime in lightly *n*-doped Ge at room temperature. We exploit the optical orientation technique<sup>28,29</sup> taking place below the edges of Pt stripes<sup>30–32</sup> to locally generate spin-polarized electrons in Ge. The spin detection is performed by measuring the voltage drop given by the inverse spin-Hall effect (ISHE) in a thin Pt pad<sup>33,34</sup> grown on Ge and spatially separated from the point where spin is generated. This nonlocal spin injection/detection scheme allows one to directly image spin transport either in the diffusive<sup>31</sup> or the drift-diffusive regime. We find that the typical decay length of the spin polarization  $L_s$  is doubled (halved) compared with the diffusive case for spin-polarized electrons flowing downstream (upstream) with respect to the applied electric field  $E = 24$  V/cm. In the best case scenario, we experimentally detect a spin loss of just the 40% within a 30  $\mu\text{m}$ -long path, corresponding to  $L_s \approx 40$   $\mu\text{m}$ . Comparable values of the spin-diffusion length in semiconductors have been predicted<sup>13,35–38</sup> and observed<sup>39</sup> only at cryogenic temperatures.

A sketch of the investigated sample is presented in Fig. 1(a). We etch a lightly *n*-doped Ge substrate (donor concentration  $N_d \approx 2 \times 10^{15} \text{ cm}^{-3}$ ) to obtain a 1  $\mu\text{m}$ -thick and 50  $\mu\text{m} \times 1$  mm-wide mesa to loosely constrain the spin transport along one direction. We then lithographically define a set of Pt stripes on the mesa surface. When illuminated, these stripes participate in the optical spin orientation process, as described below. The stripes are 10 nm-thick and  $40 \times 3 \mu\text{m}^2$ -wide, with a center-to-center pitch of 6  $\mu\text{m}$ . One of them [the first and 5  $\mu\text{m}$ -wide stripe on the left in Fig. 1(a)] is contacted with Au/Ti electrodes and serves as a spin detector. The flow of spin-polarized electrons entering this Pt detection pad is converted via the inverse spin-Hall effect (ISHE) in a charge flow, which we record as a voltage drop in open-circuit conditions across the ISHE electrodes. A  $\text{SiO}_2$  layer [green in Fig. 1(a)] below the contacts on the ISHE detector prevents direct spin and charge absorption

from the substrate. We apply a bias electric potential  $V_b$  across two AgSb Ohmic contacts<sup>40</sup> grown on Ge to generate a static electric field  $E$  in the semiconductor. For further details on sample growth and characterization, see the [supplementary material](#).

The measurements are performed at room temperature with a confocal microscope (see Ref. 31). The light source is a laser diode tuned at the direct gap of Ge ( $h\nu = 0.8$  eV) delivering an optical power equal to 270  $\mu\text{W}$ . The circular polarization of the photons is modulated at 50 kHz by means of a photoelastic modulator (PEM). An objective with 0.7 numerical aperture focuses the light on the sample with a diffraction-limited spot of  $\approx 1.3$   $\mu\text{m}$ . The measured ISHE signal  $\Delta V_{\text{ISHE}}$  is obtained by demodulating at the PEM frequency the voltage drop recorded across the Au/Ti ISHE contacts, while the laser spot raster scans the surface of the sample. The optical reflectivity of the sample is simultaneously measured with a photodetector.

In our setup, only the electrons with a component of the spin polarization directed along  $x$  [reference frame of Fig. 1(a)] give rise to a detectable  $\Delta V_{\text{ISHE}}$  (as detailed, e.g., in Ref. 25). When the light beam impinges on the edge of a metal stripe, the electromagnetic wavefront is altered<sup>30</sup> yielding a highly localized spin accumulation in the semiconductor, with a detectable in-plane positive (negative) component along the  $x$  axis below the left (right) edge of the Pt stripe. The details of the technique are reported in Refs. 30–32.

The spin-polarized electrons are generated at the  $\Gamma$  point of the Brillouin zone and within 300 fs they scatter to the  $L$  valleys, mostly preserving their spin polarization.<sup>25,41</sup> Within the explored range of applied electric fields ( $|E| < 24$  V/cm), conduction occurs at  $L$ .<sup>42,43</sup> It is worth mentioning that, together with spin-polarized electrons, a net population of spin-polarized holes is also generated via optical orientation.<sup>8</sup> However, any hole contribution to the spin current over the investigated length scales can be neglected since the

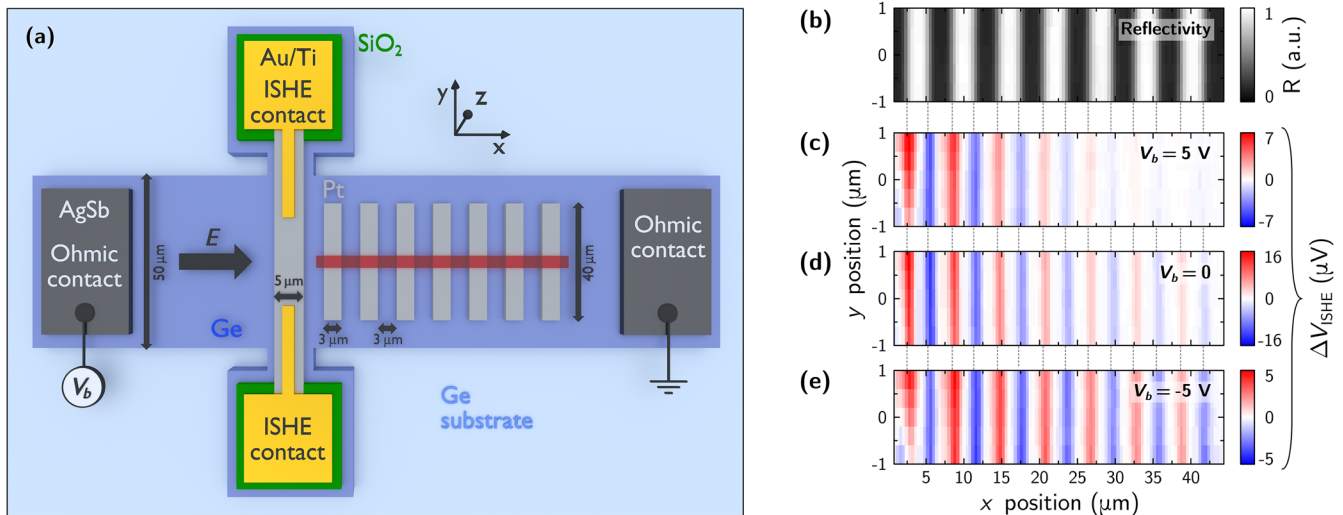


**FIG. 1.** (a) Sketch of the sample, illustrating the layout of our device (not in scale). A mesa of Ge is realized on the top of a Ge substrate. A set of Pt stripes is employed to inject in-plane spin-polarized electrons via optical orientation, while a contacted Pt stripe works as a spin detector by means of the inverse spin-Hall effect (ISHE). AgSb Ohmic contacts are exploited to generate an electrostatic field  $E$  in Ge. More details can be found in Appendix B of the [supplementary material](#). (b)–(e) Experimental data showing (b) the reflectivity map of the acquired region [highlighted in red in panel (a)] and the corresponding  $\Delta V_{\text{ISHE}}$  signal for a bias voltage ( $V_b$ ) of (c) 5 V, (d) 0 V, and (e) –5 V.

hole spin lifetime is only a few picoseconds.<sup>44</sup> This limits the spin-diffusion length of holes to few tens of nanometers in the purely diffusive regime and to—possibly—100 nm in the drift-diffusion regime. Note that the minimum distance between generation and detection points in our setup is 3  $\mu\text{m}$ . It is also worth mentioning that the presence of the Pt stripes employed in the spin-injection process is not expected to alter the spin-transport length in a significant way.<sup>31</sup>

In Figs. 1(b)–1(e), we report the experimental map acquired in the  $40 \times 2 \mu\text{m}^2$  band highlighted in red in Fig. 1(a). Due to the higher reflectivity of Pt stripes compared to the Ge substrate, the former appear bright in the reflectivity map [Fig. 1(b)]. Panels (c)–(e) show the map of the electrical signal  $\Delta V_{\text{ISHE}}$  recorded by the detector (located out of the maps at  $x = 0$ ) for three values of the bias voltage  $V_b$ . In all cases, when the light beam illuminates the left (right) edges of Pt stripes, a positive (negative)  $\Delta V_{\text{ISHE}}$  is detected, corresponding to the complementary spin populations generated in Ge below opposite Pt edges. This, together with the linear dependence of  $\Delta V_{\text{ISHE}}$  on the optical power and on the degree of circular polarization of the light (data not shown), confirms the spin-related nature of the detected signal.<sup>25</sup>

In Figs. 1(c)–1(e), the absolute value of the ISHE signal decreases with the increase in the distance of the injection point of the spin-polarized electrons, i.e., at larger  $x$  values. This is the fingerprint of the spin depolarization that electrons experience before reaching the detector. Such a decrease is less (more) pronounced for negative (positive)  $V_b$  values, corresponding to  $E_x > 0$  ( $E_x < 0$ ) [see panels (e) and (c), respectively] compared to the zero field case [panel (d)]. This indicates that the transport of spin-polarized electrons can be modulated by the application of an electric field: Depending on the field direction, electrons acquire a drift velocity and cover the distance to the ISHE detector in less (more) time, thus reducing (increasing) their loss of spin polarization. It is worth mentioning that, despite the fact that high electric fields could contribute to a faster spin depolarization, the employed  $E$  values are not expected to significantly affect the spin-relaxation time.<sup>21,45</sup>

In Fig. 2, we show the average along the  $y$  axis of the  $\Delta V_{\text{ISHE}}$  maps similar to those reported in Figs. 1(c)–1(e) for a set of positive

[panel (a)] and negative [panel (b)] bias voltages. Due to the modulation of the typical decay length of the spin-polarization—spin-transport length  $L_s$ , from now on—spin-polarized electrons generated far from the detection point are suppressed (preserved) as  $|V_b|$  increases for positive (negative) values. In the most favorable scenario, corresponding to  $V_b = -5$  V, a 30  $\mu\text{m}$ -long path reduces the  $\Delta V_{\text{ISHE}}$  signal by 40% only. Moreover,  $\Delta V_{\text{ISHE}}$  is modulated by a factor  $7 \pm 2$  when optical spin orientation is performed at the last Pt stripe ( $x \approx 40 \mu\text{m}$ ) by switching the bias voltage between  $V_b = +5$  V and  $V_b = -5$  V.

It can be noticed that in Figs. 1(c)–1(e) and 2, the maximum value of  $\Delta V_{\text{ISHE}}$  is obtained for  $V_b = 0$ . For  $V_b > 0$ , the lowering of  $\Delta V_{\text{ISHE}}$  is due to the reduction of the spin-transport length in the drift-diffusion regime. Conversely, for  $V_b < 0$ , the applied field quickly removes electrons from below the detection pad, reducing their transit time and, consequently, the probability that spin-polarized electrons are injected into the detection pad and contribute to  $\Delta V_{\text{ISHE}}$ .

We perform a quantitative analysis of the profiles in Fig. 2 by fitting the absolute value of the  $\Delta V_{\text{ISHE}}$  peaks with a function  $A e^{-x/L_s}$  that accounts for spin depolarization in the generation-to-detection path, with  $A$  being the amplitude related to the spin-sink efficiency of the detector and  $L_s$  being the spin-transport length.<sup>31</sup> For  $V_b = 0$ , the latter corresponds to the spin-diffusion length  $L_{s,0} = \sqrt{D\tau_s}$ , with  $D$  being the diffusion coefficient and  $\tau_s$  being the spin lifetime. The  $L_s$  and  $A$  values obtained from the fitting procedure are reported in Fig. 3 as a function of the applied electric field  $E_x$ . The latter has been estimated from the bias potential  $V_b$  by numerically simulating the three-dimensional field distribution in the whole structure. We obtain that a bias potential  $V_b = 1$  V yields an almost uniform electric field  $E_x = -4.75$  V/cm into the stripe. Further information about the electrical simulations is reported in the [supplementary material](#).

While the  $L_{s,0} = 20 \pm 0.5 \mu\text{m}$  value obtained at  $E_x = 0$  is comparable with previous results obtained with lightly  $n$ -doped Ge,<sup>46</sup>  $L_s$  is nearly doubled (halved) compared to  $L_{s,0}$  at  $E_x = \pm 24$  V/cm for spin-polarized electrons flowing downstream (upstream) [see panel (a)]. The largest value we obtain is  $L_s = 39 \pm 2 \mu\text{m}$ , a distance previously achieved only under cryogenic conditions.<sup>39</sup> In Fig. 3(a),

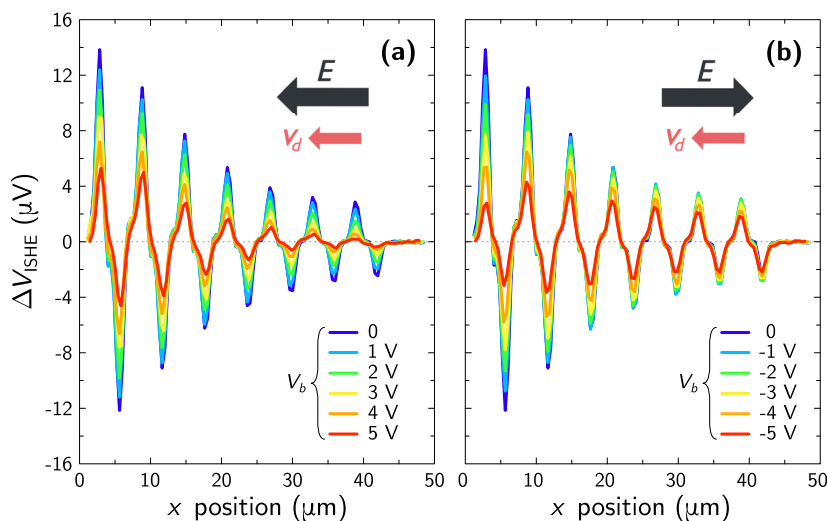


**FIG. 2.** Profiles of the ISHE signal acquired in the red band shown in Fig. 1(a) and averaged along the  $y$  axis for (a) positive and (b) negative  $V_b$  values.  $E$  and  $v_d$  arrows represent the direction of the electric field and the spin-diffusion velocity, respectively. The experimental error of  $\Delta V_{\text{ISHE}}$  at the first stripe for  $V_b$  ranging from  $-3$  to  $-5$  V is much larger than the ones obtained by illuminating at other  $x$  positions and for different bias values. Note that all the experimental data are acquired with the same optical power (equal to 270  $\mu\text{W}$ ).

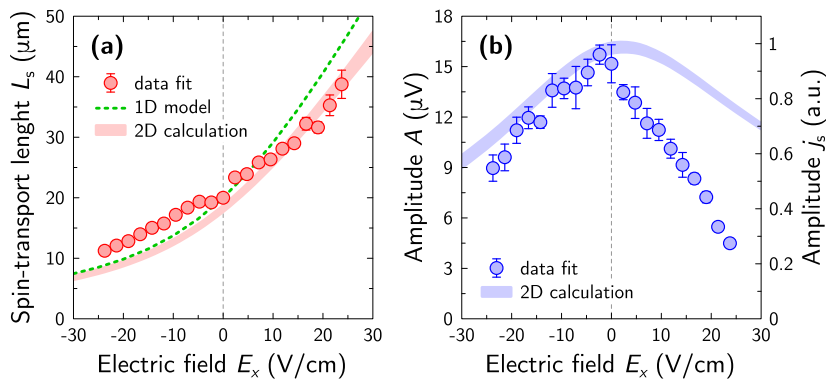


**FIG. 3.** (a) Spin-transport length  $L_s$  and (b) amplitude related to spin-sink efficiency  $A$  (see text) obtained from the fitting of experimental profiles similar to the ones reported in Fig. 2. The green dotted line in panel (a) represents the spin-transport length predicted by the analytical one-dimensional spin drift-diffusion model [Eq. (1)]. The thick lines represent the results of two-dimensional numerical simulations (see text).

the experimentally inferred  $L_s$  values are compared to the spin-transport length obtained from the analytical solution of the one-dimensional (1D) coupled spin continuity and spin drift-diffusion equations (green dotted line, details are given in the [supplementary material](#)),<sup>21,47</sup>

$$L_s = \left[ -\frac{1}{2} \frac{eE_x}{k_B T} + \sqrt{\left( \frac{1}{2} \frac{eE_x}{k_B T} \right)^2 + \frac{1}{L_{s,0}^2}} \right]^{-1}, \quad (1)$$

with  $k_B$  being the Boltzmann constant,  $e$  being the elementary charge, and  $T$  being the lattice temperature. Equation (1) well reproduces the experimental  $L_s$  vs  $E_x$  trend reported in Fig. 3(a). In the [supplementary material](#), we derive the conditions at which a sizeable modulation of the spin signal occurs. The key ingredients are a finite spin-diffusion length  $L_{s,0}$ , which needs to be comparable to the device length, and electric fields  $|E_x| \lesssim 2k_B T/(eL_{s,0})$ . Equation (1) also allows predicting the dependence of the spin-transport length  $L_s$  on the doping concentration. The latter affects  $L_s$  by influencing the spin-diffusion length  $L_{s,0}$ , which can be addressed either experimentally<sup>4,46</sup> or theoretically.<sup>4,13,25</sup>

To better understand the role of geometry in our device, we performed two-dimensional (2D) finite-element spin-transport simulations on the  $xz$  plane in Fig. 1(a). To keep the numerical simulations as simple as possible, we assumed a uniform electric field directed along  $x$  (details are given in the [supplementary material](#)). We then estimated the spin current density  $j_s$  entering the Pt detector, which is proportional to the experimentally measured  $\Delta V_{\text{ISHE}}$  value.<sup>48</sup> Compared to the 1D model, the 2D simulations slightly improve the agreement with the experimentally inferred  $L_s$  value at positive  $E$ , as shown by the thick line in Fig. 3(a). The difference between the theoretical and experimental values of  $L_s$  is lower than  $2 \mu\text{m}$  within the whole explored range of applied electric fields.

The 2D simulations also qualitatively reproduce the trend of the experimentally determined amplitude  $A$  [Fig. 3(b)], confirming the reduction of  $A$  both for positive and negative applied fields, as a consequence of the variation of the spin-diffusion length for  $E_x < 0$  and of the transit time of spin-polarized electrons below the detection pad for  $E_x > 0$ . The main discrepancy between experimental data and 2D simulations is that the latter underestimate the decrease of  $A$  for  $E_x > 0$ . We ascribe this deviation to the presence of a  $z$  component of the electric field (not accounted for in the simulations), which modifies the built-in electric field of the Pt/Ge junction and

thus modulates the transmission efficiency of electrons through the Schottky barrier.<sup>49</sup> We stress, however, that 2D simulations capture the fundamental physical mechanisms underpinning spin-transport.

In conclusion, we have directly imaged the transport of spin-polarized electrons in Ge in either the diffusive or drift-diffusive regime. We experimentally demonstrate that, thanks to the finite spin lifetime, an electric field can strongly modulate the distance traveled by spin carriers before they depolarize. In this way, we are able to modulate by about one order of magnitude the spin-polarized electrons reaching the detector. The largest spin-transport length we measure is  $40 \mu\text{m}$ , which in a purely diffusive regime can only be attained at cryogenic temperatures. Model predictions are in agreement with the experimental findings. Our results open the route to the exploitation of electric fields for guiding and controlling spins across spintronic devices.

See the [supplementary material](#) for details about sample micro-fabrication, electrical simulations, spin drift-diffusion models (1D and 2D), and modulation of spin accumulation.

## AUTHOR DECLARATIONS

### Conflict of Interest

The authors declare no conflict of interest.

### DATA AVAILABILITY

The data that support the findings of this study are available from the corresponding author upon reasonable request.

## REFERENCES

- D. D. Awschalom and M. E. Flatté, "Challenges for semiconductor spintronics," *Nat. Phys.* **3**, 153–159 (2007).
- J. Fabian, A. Matos-Abiague, C. Ertler, P. Stano, and I. Žutić, "Semiconductor spintronics," *Acta Phys. Slovaca* **57**, 565 (2007).
- A. Manchon, H. C. Koo, J. Nitta, S. M. Frolov, and R. A. Duine, "New perspectives for Rashba spin-orbit coupling," *Nat. Mater.* **14**, 871–882 (2015).
- K. Hamaya, Y. Fujita, M. Yamada, M. Kawano, S. Yamada, and K. Sawano, "Spin transport and relaxation in germanium," *J. Phys. D: Appl. Phys.* **51**, 393001 (2018).
- T. F. Watson, B. Weber, Y.-L. Hsueh, L. C. L. Hollenberg, R. Rahman, and M. Y. Simmons, "Atomically engineered electron spin lifetimes of 30 s in silicon," *Sci. Adv.* **3**, 1602811 (2017).
- F. Dirnberger, M. Kammermeier, J. König, M. Forsch, P. E. Faria Junior, T. Campos, J. Fabian, J. Schliemann, C. Schüller, T. Korn, P. Wenk, and D. Bougeard,

- <sup>4</sup>“Ultralong spin lifetimes in one-dimensional semiconductor nanowires,” *Appl. Phys. Lett.* **114**, 202101 (2019).
- <sup>7</sup>M. Dyakonov and V. Perel, “Spin relaxation of conduction electrons in noncentrosymmetric semiconductors,” *Sov. Phys. Solid State* **13**, 3023–3026 (1972).
- <sup>8</sup>J. Rioux and J. E. Sipe, “Optical injection and control in germanium: Thirty-band  $\mathbf{k} \cdot \mathbf{p}$  theory,” *Phys. Rev. B* **81**, 155215 (2010).
- <sup>9</sup>J. L. Cheng, J. Rioux, J. Fabian, and J. E. Sipe, “Theory of optical spin orientation in silicon,” *Phys. Rev. B* **83**, 165211 (2011); [arXiv:1011.2259](https://arxiv.org/abs/1011.2259).
- <sup>10</sup>M. Hochberg and T. Baehr-Jones, “Towards fabless silicon photonics,” *Nat. Photonics* **4**, 492–494 (2010).
- <sup>11</sup>M. J. Süess, R. Geiger, R. A. Minamisawa, G. Schiefler, J. Frigerio, D. Chrastina, G. Isella, R. Spolenak, J. Faist, and H. Sigg, “Analysis of enhanced light emission from highly strained germanium microbridges,” *Nat. Photonics* **7**, 466–472 (2013).
- <sup>12</sup>F. Bottegoni, G. Isella, S. Cecchi, and F. Ciccacci, “Spin polarized photoemission from strained Ge epilayers,” *Appl. Phys. Lett.* **98**, 242107 (2011).
- <sup>13</sup>P. Li, Y. Song, and H. Dery, “Intrinsic spin lifetime of conduction electrons in germanium,” *Phys. Rev. B* **86**, 085202 (2012).
- <sup>14</sup>M. Bollani, D. Chrastina, L. Gagliano, L. Rossetto, D. Scopece, M. Barget, V. Mondiali, J. Frigerio, M. Lodari, F. Pezzoli, F. Montalenti, and E. Bonera, “Local uniaxial tensile strain in germanium of up to 4% induced by SiGe epitaxial nanostructures,” *Appl. Phys. Lett.* **107**, 083101 (2015).
- <sup>15</sup>S. A. Crooker and D. L. Smith, “Imaging spin flows in semiconductors subject to electric, magnetic, and strain fields,” *Phys. Rev. Lett.* **94**, 236601 (2005).
- <sup>16</sup>T. Sasaki, Y. Ando, M. Kameno, T. Tahara, H. Koike, T. Oikawa, T. Suzuki, and M. Shiraishi, “Spin transport in nondegenerate Si with a spin MOSFET structure at room temperature,” *Phys. Rev. Appl.* **2**, 034005 (2014).
- <sup>17</sup>A. Spiesser, Y. Fujita, H. Saito, S. Yamada, K. Hamaya, W. Mizubayashi, K. Endo, S. Yuasa, and R. Jansen, “Quantification of spin drift in devices with a heavily doped Si channel,” *Phys. Rev. Appl.* **11**, 044020 (2019).
- <sup>18</sup>M. Kameno, Y. Ando, T. Shinjo, H. Koike, T. Sasaki, T. Oikawa, T. Suzuki, and M. Shiraishi, “Spin drift in highly doped n-type Si,” *Appl. Phys. Lett.* **104**, 092409 (2014).
- <sup>19</sup>T. Tahara, Y. Ando, M. Kameno, H. Koike, K. Tanaka, S. Miwa, Y. Suzuki, T. Sasaki, T. Oikawa, and M. Shiraishi, “Observation of large spin accumulation voltages in nondegenerate Si spin devices due to spin drift effect: Experiments and theory,” *Phys. Rev. B* **93**, 214406 (2016).
- <sup>20</sup>J. H. Kwon, H. C. Koo, J. Eom, J. Chang, and S.-H. Han, “Electric field effect on spin diffusion in a semiconductor channel,” *IEEE Trans. Magn.* **44**, 2647–2650 (2008).
- <sup>21</sup>Z. G. Yu and M. E. Flatté, “Electric-field dependent spin diffusion and spin injection into semiconductors,” *Phys. Rev. B* **66**, 201202(R) (2002).
- <sup>22</sup>A. T. Hanbicki, B. T. Jonker, G. Itskos, G. Kioseoglou, and A. Petrou, “Efficient electrical spin injection from a magnetic metal/tunnel barrier contact into a semiconductor,” *Appl. Phys. Lett.* **80**, 1240–1242 (2002).
- <sup>23</sup>C. Józsa, M. Popinciu, N. Tombros, H. T. Jonkman, and B. J. van Wees, “Electronic spin drift in graphene field-effect transistors,” *Phys. Rev. Lett.* **100**, 236603 (2008).
- <sup>24</sup>G. Wang, B. L. Liu, A. Balocchi, P. Renucci, C. R. Zhu, T. Amand, C. Fontaine, and X. Marie, “Gate control of the electron spin-diffusion length in semiconductor quantum wells,” *Nat. Commun.* **4**, 2372 (2013).
- <sup>25</sup>C. Zucchetti, F. Bottegoni, G. Isella, M. Finazzi, F. Rortais, C. Vergnaud, J. Widiez, M. Jamet, and F. Ciccacci, “Spin-to-charge conversion for hot photoexcited electrons in germanium,” *Phys. Rev. B* **97**, 125203 (2018).
- <sup>26</sup>F. Bottegoni, C. Zucchetti, G. Isella, M. Bollani, M. Finazzi, and F. Ciccacci, “Spin-charge interconversion in heterostructures based on group-IV semiconductors,” *Riv. Nuovo Cimento* **43**, 45 (2020).
- <sup>27</sup>H. Dery, P. Dalal, L. Cywiński, and L. J. Sham, “Spin-based logic in semiconductors for reconfigurable large-scale circuits,” *Nature* **447**, 573–576 (2007).
- <sup>28</sup>G. Lampel, “Nuclear dynamic polarization by optical electronic saturation and optical pumping in semiconductors,” *Phys. Rev. Lett.* **20**, 491–493 (1968).
- <sup>29</sup>F. Meier and B. P. Zakharchenya, *Optical Orientation* (Elsevier, 1984).
- <sup>30</sup>F. Bottegoni, M. Celebrano, M. Bollani, P. Biagioni, G. Isella, F. Ciccacci, and M. Finazzi, “Spin voltage generation through optical excitation of complementary spin populations,” *Nat. Mater.* **13**, 790–795 (2014).
- <sup>31</sup>C. Zucchetti, F. Bottegoni, C. Vergnaud, F. Ciccacci, G. Isella, L. Ghirardini, M. Celebrano, F. Rortais, A. Ferrari, A. Marty, M. Finazzi, and M. Jamet, “Imaging spin diffusion in germanium at room temperature,” *Phys. Rev. B* **96**, 014403 (2017).
- <sup>32</sup>T. Guillet, C. Zucchetti, A. Marchionni, A. Hallal, P. Biagioni, C. Vergnaud, A. Marty, H. Okuno, A. Masseboeuf, M. Finazzi, F. Ciccacci, M. Chshiev, F. Bottegoni, and M. Jamet, “Spin orbitronics at a topological insulator-semiconductor interface,” *Phys. Rev. B* **101**, 184406 (2020).
- <sup>33</sup>M. Dyakonov and V. Perel, “Possibility of orienting electrons spins with current,” *JETP Lett.* **13**, 467–469 (1971).
- <sup>34</sup>M. I. Dyakonov and V. I. Perel, “Current-induced spin orientation of electrons in semiconductors,” *Phys. Lett. A* **35**, 459–460 (1971).
- <sup>35</sup>J. L. Cheng, M. W. Wu, and J. Fabian, “Theory of the spin relaxation of conduction electrons in silicon,” *Phys. Rev. Lett.* **104**, 016601 (2010).
- <sup>36</sup>P. Li and H. Dery, “Spin-orbit symmetries of conduction electrons in silicon,” *Phys. Rev. Lett.* **107**, 107203 (2011).
- <sup>37</sup>Y. Song and H. Dery, “Analysis of phonon-induced spin relaxation processes in silicon,” *Phys. Rev. B* **86**, 085201 (2012).
- <sup>38</sup>M. Finazzi, F. Bottegoni, C. Zucchetti, M. Bollani, A. Ballabio, J. Frigerio, F. Rortais, C. Vergnaud, A. Marty, M. Jamet, G. Isella, and F. Ciccacci, “Optical orientation and inverse spin Hall effect as effective tools to investigate spin-dependent diffusion,” *Electronics* **5**, 80 (2016).
- <sup>39</sup>F. Bottegoni, C. Zucchetti, S. Dal Conte, J. Frigerio, E. Carpena, C. Vergnaud, M. Jamet, G. Isella, F. Ciccacci, G. Cerullo, and M. Finazzi, “Spin-Hall voltage over a large length scale in bulk germanium,” *Phys. Rev. Lett.* **118**, 167402 (2017).
- <sup>40</sup>D. C. S. Dumas, K. Gallacher, R. Millar, I. MacLaren, M. Myronov, D. R. Leadley, and D. J. Paul, “Silver antimony Ohmic contacts to moderately doped n-type germanium,” *Appl. Phys. Lett.* **104**, 162101 (2014).
- <sup>41</sup>F. Pezzoli, F. Bottegoni, D. Trivedi, F. Ciccacci, A. Giorgioni, P. Li, S. Cecchi, E. Grilli, Y. Song, M. Guzzi, H. Dery, and G. Isella, “Optical spin injection and spin lifetime in Ge heterostructures,” *Phys. Rev. Lett.* **108**, 156603 (2012).
- <sup>42</sup>J. B. Gunn, “Instabilities of current in III-V semiconductors,” *IBM J. Res. Dev.* **8**, 141–159 (1964).
- <sup>43</sup>N. Okamoto, H. Kurebayashi, T. Trypiniotis, I. Farrer, D. A. Ritchie, E. Saitoh, J. Sinova, J. Mašek, T. Jungwirth, and C. H. W. Barnes, “Electric control of the spin Hall effect by intervalley transitions,” *Nat. Mater.* **13**, 932–937 (2014).
- <sup>44</sup>F. Rortais, S. Oyarzún, F. Bottegoni, J.-C. Rojas-Sánchez, P. Laczkowski, A. Ferrari, C. Vergnaud, C. Ducruet, C. Beigné, N. Reyren, A. Marty, J.-P. Attané, L. Vila, S. Gambarelli, J. Widiez, F. Ciccacci, H. Jaffrès, J.-M. George, and M. Jamet, “Spin transport in p-type germanium,” *J. Phys.: Condens. Matter* **28**, 165801 (2016).
- <sup>45</sup>J. Li, L. Qing, H. Dery, and I. Appelbaum, “Field-induced negative differential spin lifetime in silicon,” *Phys. Rev. Lett.* **108**, 157201 (2012).
- <sup>46</sup>C. Zucchetti, M. Bollani, G. Isella, M. Zani, M. Finazzi, and F. Bottegoni, “Doping dependence of the electron spin diffusion length in germanium,” *APL Mater.* **7**, 101122 (2019).
- <sup>47</sup>M. I. Miah, “Drift-diffusion crossover and the intrinsic spin diffusion lengths in semiconductors,” *J. Appl. Phys.* **103**, 063718 (2008).
- <sup>48</sup>K. Ando, M. Morikawa, T. Trypiniotis, Y. Fujikawa, C. H. W. Barnes, and E. Saitoh, “Direct conversion of light-polarization information into electric voltage using photoinduced inverse spin-Hall effect in Pt/GeAs hybrid structure: Spin photodetector,” *J. Appl. Phys.* **107**, 113902 (2010).
- <sup>49</sup>C. Zucchetti, G. Isella, F. Ciccacci, M. Finazzi, and F. Bottegoni, “Spin transport and spin-charge interconversion phenomena in Ge-based structures,” *Proc. SPIE* **11090**, 1109033 (2019).